2D Raman band of single-layer and bilayer graphene

2016 J. Phys.: Conf. Ser. 682 012013

(http://iopscience.iop.org/1742-6596/682/1/012013)

2D Raman band of single-layer and bilayer graphene

V N Popov
Faculty of Physics, University of Sofia, BG-1164 Sofia, Bulgaria

E-mail: vpopov@phys.uni-sofia.bg

Abstract. We present a computational study of the 2D Raman band of single-layer and bilayer graphene within a density-functional-based non-orthogonal tight-binding model. The phonon dispersion is derived perturbatively and the 2D band intensity is calculated in fourth-order quantum perturbation theory within this model. The 2D band intensity is enhanced through resonant processes in which the laser excitation matches an electronic transition and the energy and momentum of the scattered phonons match the difference of those of pairs of electronic states. As a result, the 2D band is dispersive, i.e., its position depends on the laser excitation. Here, we calculate the shift and shape, as well as the dispersion rate, of the 2D band for both single-layer graphene and bilayer graphene. The results are compared to available experimental data.

1. Introduction

The successful synthesis of few-layer graphene [1] and the theoretical predictions of its amazing electronic properties[2,3] have triggered an avalanche of theoretical and experimental work. Few-layer graphene has been identified as a promising material with prospective application in nanoelectronics [4].Various experimental techniques are currently applied to the characterization of the few-layer samples but Raman spectroscopy has obvious advantages as an inexpensive and nondestructive technique of choice [5].

Few-layer graphene is a two-dimensional structure of stacked graphene layers. In the simplest case of a single-layer graphene (SLG), there is only one Raman-active phonon, which gives rise to the G band in the Raman spectra. In perfect graphene, the latter are dominated by the two-phonon 2D band, which is several times more intense than the G band. The 2D band is observed because of resonant processes and is, therefore, *dispersive*, meaning dependence of the Raman band position on the laser excitation. The theoretical description of these resonant processes has been proposed more than a decade ago [6], but realistic calculations of the position, line shape, and dispersion rate of SLG have been reported only recently [7,8].

The bilayer graphene (BLG) consists of two graphene layers with either AA, or AB stacking. Most efforts have been applied to the study of the more stable AB-stacked structure. The two layers are bound together by weak Van der Waals interactions, resulting in splitting of the doubled electron and phonon dispersions. Although the splitting is comparatively small, the split components of an electronic band or phonon branch have different symmetries, yielding modified resonant processes for the 2D band. Recently, the calculated 2D band of BLG has been reported [9] and a systematic study of the two-phonon Raman bands of BLG and their dispersion rates has been performed [10]. While a significant amount of work has already been done on the clarification of the underlying scattering processes, a comparative investigation of these processes and the calculated 2D bands is still lacking.

Here, we report a comparative study of the 2D band of SLG and BLG, revealing the similarities and differences in the resonant processes, responsible for these bands.

2. Theoretical

The electronic band structure is calculated here within a density-functional-based non-orthogonal tight-binding model (NTB) [11]. The dependence of the Hamiltonian and overlap matrix elements on the radial coordinate is taken over from ab-initio studies on carbon dimers [12,13].Only matrix elements between atomic orbitals of type s, p_x, p_y, p_z are considered. The Slater – Koster scheme is used for the angular dependence of the matrix elements. The model is appended with repulsive potentials, also derived within the ab-initio approach. The total repulsive energy describes part of the electronic correlations, which is not included in the band energy. The possibility to calculate the total energy allows for performing relaxation of the atomic structure. This step is indispensable for phonon dispersion calculations.

The phonon dispersion is calculated using a perturbative approach within the NTB model [14]. This approach makes utilizes electron-phonon matrix elements, which are derived within the NTB model [15]. The Raman intensity *I* of any two-phonon Raman band can be calculated in fourth-order perturbation theory within the NTB model by use of the expression [8,10]:

$$I \propto \sum_f \left| \sum_{c,b,a} \frac{M_{fc} M_{cb} M_{ba} M_{ai}}{\Delta E_{ic} \Delta E_{ib} \Delta E_{ia}} \right|^2 \delta\left(E_i - E_f\right) . \quad (1)$$

Here, $E_{iu} = E_u - E_i$, where $E_u (u = a, b, c)$ are the energies of the intermediate states of the system of photons, electrons, holes, and phonons. E_i is the initial state energy, equal to the laser excitation energy E_L. M_{ai} and M_{fc} are the momentum matrix elements for creation and recombination of an electron-hole pair, respectively. M_{ba} and M_{cb} are the electron-phonon matrix elements for scattering between intermediate states. The electron-photon and electron-phonon matrix elements are calculated explicitly within the NTB model [15]. The summation over the intermediate states runs over all valence and conduction bands, and over all electron wavevectors **k**. The summation over the final states runs over the considered pair of phonon branches and over all phonon wavevectors **q**. For both summations, convergence is reached with a 400 × 400 mesh of **k** and **q** points in the Brillouin zone. The calculations are performed for parallel scattering configuration, backscattering geometry, and Stokes processes.

3. Results and discussion

The atomic structure of AB-stacked BLG is shown in figure 1. It has a unit cell of four atoms, while the unit cell of SLG has only two atoms. Both structures have hexagonal symmetry and share a common Brillouin zone (figure 1).

The electron dispersion is readily derived by solving the non-orthogonal tight-binding equation of rank equal to the product of the number of atoms per unit cell (2 or 4) and the number of atomic orbitals per atom (4). The calculated electron dispersion of SLG and BLG close to the Fermi energy, taken as zero, is shown in figure 2 and figure 3, respectively. In the energy range of ±1.5 eV only π bands are present. In the case of SLG, these orbitals cross at the Fermi energy, forming a valence band (π band) and a conduction band (π* band). It is most amazing that the π bands have linear dispersion in the vicinity of the Fermi energy at the two non-equivalent special points K and K', and therefore the effective mass of the electrons is zero. This results in an effective wave equation of the Dirac – Weil type, which is often used in the simplified description of transport and optical phenomena. Away from the Fermi energy, there is a deviation from the linear behavior of the bands, known as band warping effect. The conduction and valence bands form cones above and below the plane of the two-

dimensional wavevectors, called *Dirac cones*, and the common points of these cones are called *Dirac points*.

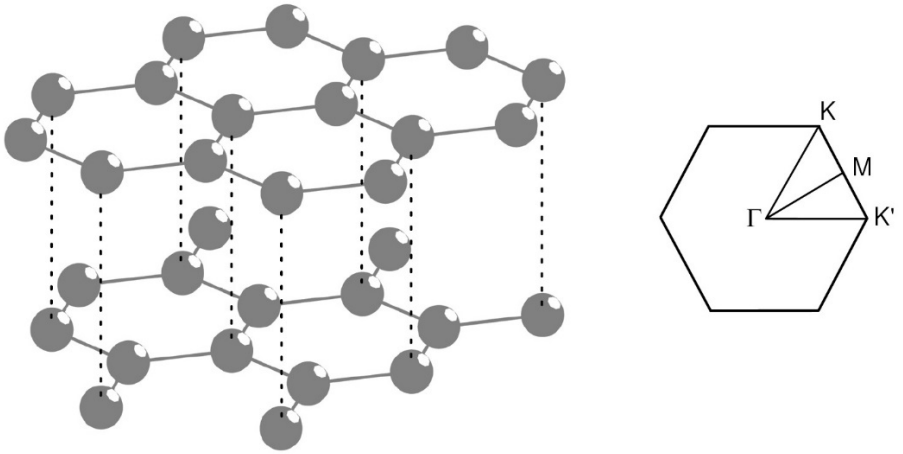

Figure 1. Left: The atomic structure of BLG consisting of two AB-stacked layers of SLG. Right: The Brillouin zone of SLG and BLG with special points.

BLG consists of two SLG layers, bound together by weak Van der Waals interactions. In the approximation of negligible interlayer interactions, the electronic dispersion of BLG is identical to that of SLG with the only difference that the number of electronic states is doubled. The account for the interlayer interactions leads to splitting of this double degeneracy of the energy levels (figure 3). However, there is a qualitative difference of the behavior of the bands of the two structures close to the Dirac points. Namely, the linear dispersion disappears and the split bands acquire parabolic wavevector dependence. This qualitatively different behavior of the bands is important at small excitations, e.g., for transport phenomena, but plays almost no role at higher energy excitations, e.g., optical phenomena. In the latter case, the most important feature is the band splitting.

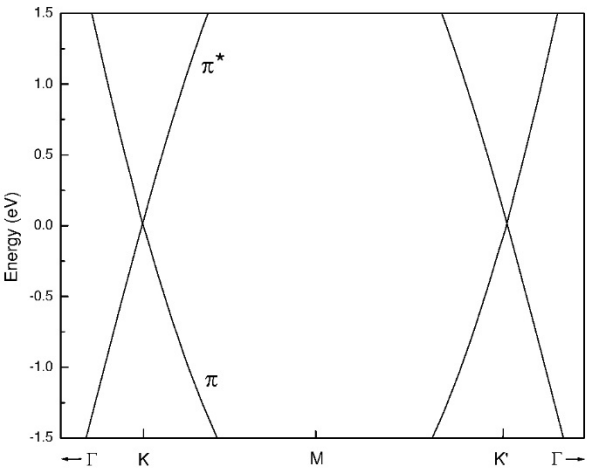

Figure 2. Electronic band structure of SLG along the KMK' direction close to the Fermi energy.

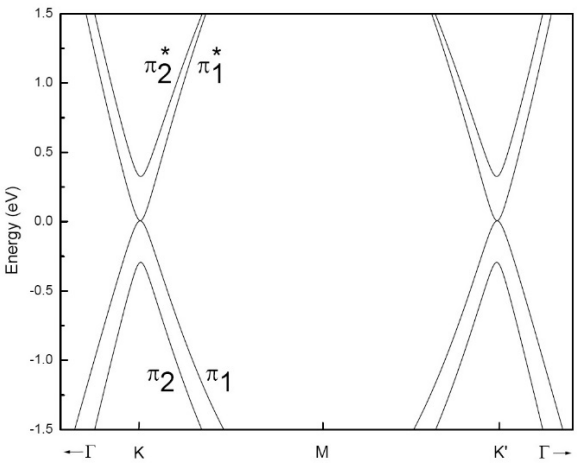

Figure 3. Electronic band structure of BLG along the KMK' direction close to the Fermi energy.

The phonon dispersion is obtained from the dynamical equation for the two structures. This equation is a matrix equation of rank equal to the product of three and the number of atoms in the unit cell (2 or 4). The calculated phonon dispersion of SLG and BLG is shown in figure 4 and figure 5, respectively. The dispersion has a number of phonon branches, denoted according to the atomic vibrational pattern. The usual notation includes the letters "L", "T", and "Z" for longitudinal, transverse, and out-of-plane, respectively. The second letter "A" and "O" denotes acoustic and optical, respectively. In BLG, the number of branches doubles in comparison with SLG and the superscript "+" and "–" is added for the branch withsymmetric and antisymmetric atomic displacement with respect to the center of symmetry, respectively. The splitting of the branches, due to interlayer interactions, is normally of about few cm^{-1}. Larger splitting is present for the ZA branch, but it is not important for the current study of the 2D band, which originates from the TO branch.

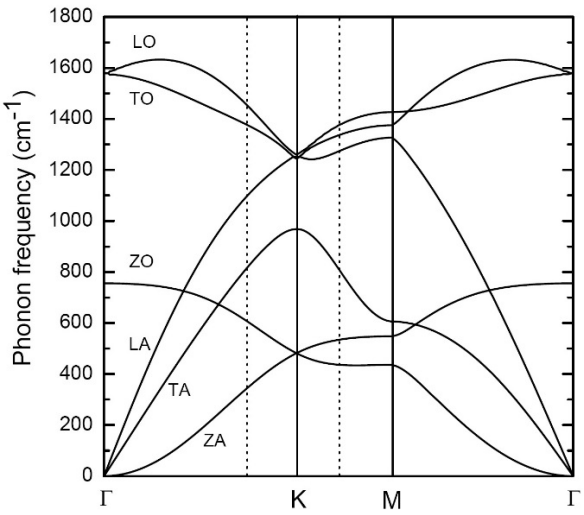

Figure 4. Phonon dispersion of SLG with the displacement pattern of the branches.

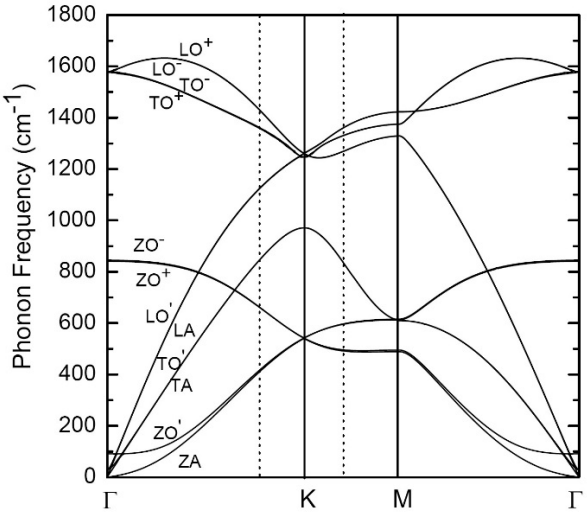

Figure 5. Phonon dispersion of BLG with the displacement pattern of the branches.

The electron and phonon dispersions are both important for the calculation of the 2D band intensity, as it is clearly seen from equation 1. In order to analyze the results, obtained by using this equation, we remind that expression inside the absolute value symbol is the scattering amplitude. The latter can be represented by a corresponding diagram, consisting of virtual processes. In the present case, the scattering process can be interpreted as a sequence of the following virtual processes: electron-hole creation, scattering of an electron (or a hole) by a phonon, a consecutive scattering of an electron (or a hole) by a phonon with opposite momentum with regard to the first phonon, and final electron-hole annihilation. There are altogether eight such scattering processes. For optical processes, the only available electronic states for scattering are those of one and the same Dirac cone at the K or K' point (intravalley processes) and those of Dirac cones at the K and K' points (intervalley processes). In this paper, all types of scattering processes are considered. A simplified schematic of one of the eight scattering processes in SLG and BLG is displayed in figure 6 and figure 7, respectively.

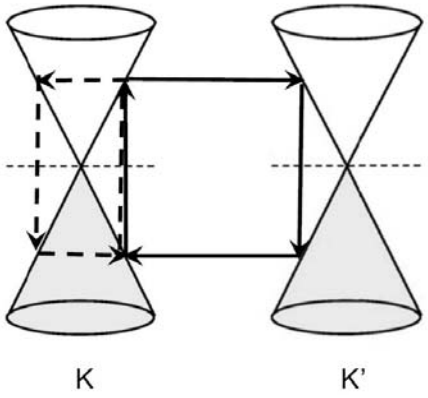

Figure 6. Dirac cones of SLG with examples of two scattering processes, drawn by dashed and solid lines in the cases of intravalley and intervalley virtual processes, respectively.

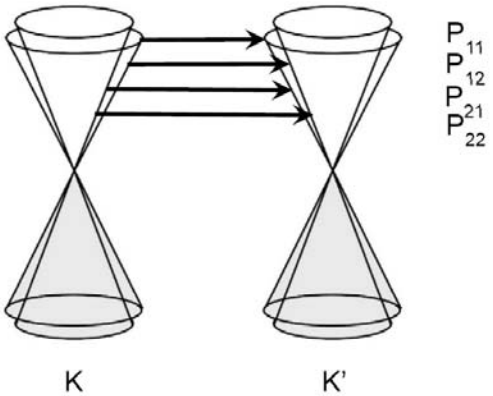

Figure 7. Dirac cones of BLG with illustration of the four types of virtual processes of electron scattering by a phonon.

In the case of BLG, the number of Dirac cones doubles and there are already four types of electron scattering processes instead of only one in SLG, as seen in figure 7. All these processes are symmetry-allowed. The following notation for these processes is adopted: P_{11}, P_{12}, P_{21}, and P_{22} (see figure 7). The doubling of the number of the Dirac cones increases the number of the electron excitation processes four times ($\pi_1 \to \pi_1^*, \pi_1 \to \pi_2^*, \pi_2 \to \pi_1^*$, and $\pi_2 \to \pi_2^*$). However, only the first and the fourth of them are symmetry-allowed. All allowed scattering processes are taken into account in the present calculation.

Looking back at equation 1, it is straightforward to perceive that some of the scattering processes will have resonant contribution to the Raman intensity for vanishing denominator of this equation. This is possible if one, two, or three of the differences $E_{iu} = E_u - E_i$ vanish. Such resonances are usually termed single, double, triple resonance. The explicit calculations show that the dominant contribution to the intensity comes from triple resonances [7,8,10].

Equation 1 can be used to obtain all two-phonon Raman bands arising from phonons with opposite momenta of all pairs of phonon branches. Bands, due to pairs from the same branch, are termed *overtone bands*, while bands, due to pairs of phonons from different branches, are *combination bands*. The intensity of a given two-phonon band depends crucially on the matrix elements in the numerator of equation 1 with the major factor determining the intensity being the electron-phonon matrix element. It has been argued that the phonons of the TO branch in the vicinity of the K and K' point have the largest electron-phonon coupling [7]. Therefore, it can be expected that the 2TO overtone and combination bands will dominate the second-order Raman spectra. This is indeed the case and the most intense band is the 2D band, which consists of these bands. The remaining, less intense two-phonon bands are discussed elsewhere [7,8,10].

The calculated 2D bands of SLG at $E_L = 1.96$ eV and BLG at $E_L = 2.33$ eV are shown in figure 8 and figure 9, respectively. The 2D band of SLG is almost symmetric in shape. The reason for the slight asymmetry of this band is due to the two types of contributions to this band. The calculations reveal that these two contributions come from TO phonons along the ΓK and KM directions. The former contribution yields about 90% of the integrated 2D band intensity. The approximate symmetry of the 2D band is due to the approximate mirror symmetry of the TO branches with respect to the K point. The increasing deviation from this symmetry with increasing the laser excitation brings about visually asymmetric 2D band shape [7,8]. The 2D band of BLG usually has an asymmetric shape because of the various contribution to this band [9,10]. The quantitative prediction of this band has

been a long-standing problem. Initially, it has been assumed that the four types of scattering processes P_{11}, P_{12}, P_{21}, and P_{22} give rise to contributions with well-resolved Raman shift and the dispersion rates of the four components of the 2D band have been derived [16]. Recently, it has been argued that the contributions of processes P_{12} and P_{21} cannot be resolved and that the experimental 2D bands should be fitted only by three Lorentzians [9,10]. The results, presented in figure 9 confirm this conclusion. It can also be seen in figure 9 that the phonon branches $TO^{\pm}$ give rise to two overtone bands $2TO^{+}$ and $2TO^{-}$ and a combination band $TO^{-}TO^{+}$, all of them being of comparable intensity but of different shape. The combination band has been overlooked in Ref.[9] resulting is a slightly different band shape.

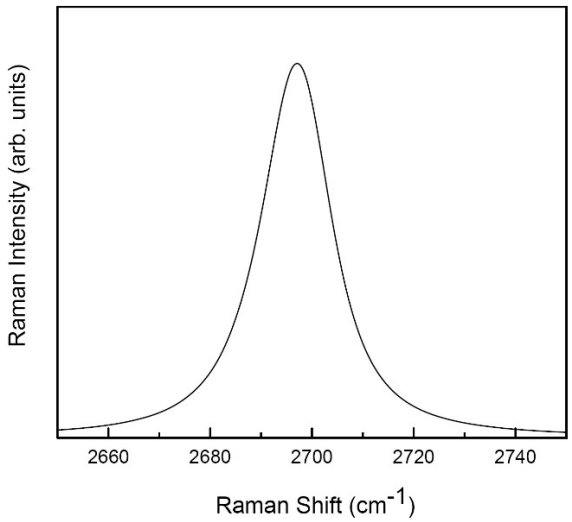

Figure 8. 2D band of SLG at EL = 1.96 eV.

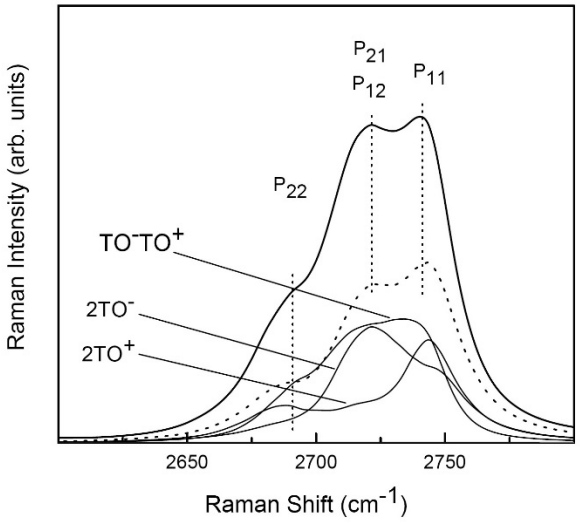

Figure 9. 2D band of BLG at EL = 2.33 eV.

Finally, the 2D band position of SLG and BLG has a clear dependence on the laser excitation (not shown). In the case of SLG, the calculated dispersion rate of89 eV/cm^{-1} agrees well with the experimental values [7]. The three components of the 2D band of BLG were found here to have close values of the dispersion rate with an average value of98 eV/cm^{-1}, which is higher than the experimental value by a few percent [5].

The reported results on the 2D Raman band of SLG and BLG can be used in the characterization of few-layer graphene. The theoretical prediction of the two-phonon bands will further facilitate the characterization of graphene samples.

Acknowledgments
The author would like to acknowledge the financial support from EU Seventh Framework Programme project INERA under grant agreement number 316309.

References

[1] GeimA K and NovoselovK S 2007 *Nature Materials***6** 183
[2] Castro Neto AH, Guinea F, Peres NMR, Novoselov KS and Geim A K 2009*Rev. Mod. Phys*. **81** 109
[3] McCann E and Koshino M 2013*Rep. Prog. Phys*.**76** 056503
[4] BonaccorsoF, SunZ, HasanT and FerrariA C 2010 *Nature Photonics***4** 611
[5] MalardL M, PimentaM A, DresselhausG and DresselhausM S 2009 *Phys. Rep*. **473** 51
[6] ThomsenC and ReichS 2000*Phys. Rev. Lett*. **85** 5214

[7] VenezuelaP, LazzeriM and MauriF 2011*Phys. Rev*. B **84** 035433
[8] Popov V N and LambinPh 2012 *Eur. Phys. J*. B **85** 418
[9] Herziger F, Calandra M, Gava P, May P, Lazzeri M, Mauri F and Maultzsch J.2014 *Phys. Rev. Lett.***113** 187401
[10] PopovV N 2015 *Carbon***91** 436
[11] PopovV N and HenrardL 2004 *Phys. Rev*. B **70** 115407
[12] PorezagD, FrauenheimT, KöhlerT, SeifertG and Kaschner R1995 *Phys. Rev*. B **51** 12947
[13] Popov V N and Van Alsenoy Ch 2014*Phys. Rev.* B **90** 245429
[14] PopovV N and LambinPh 2006 *Phys. Rev*. B **73** 085407
[15] Popov VN, Henrard L and Lambin Ph 2005*Phys. Rev*.**72**035436
[16] Malard LM, Nilsson J, Elias DC, Brant JC, Plentz F, Alves ES, Castro NetoA H and Pimenta M A2007 *Phys. Rev*. B**76** 201401(R)